Kinematic Model of a Magnetic-Microrobot Swarm in a Rotating Magnetic Dipole Field

BhanuKiran Chaluvadi, Kristen M. Stewart, Adam J. Sperry, Henry C. Fu, and Jake J. Abbott

***Abstract*—This letter describes how a rotating magnetic dipole field will manipulate the location and shape of a swarm of magnetic microrobots, specifically microrobots that convert rotation into forward propulsion, such as helical swimmers and screws. The analysis assumes a swarm that can be described by a centroid and a covariance matrix, with the swarm comprising an arbitrary and unknown number of homogenous microrobots. The result of this letter is a kinematic model that can be used as an *a priori* model for motion planners and feedback control systems. Because the model is fully three-dimensional and does not require any localization information beyond what could realistically be determined from medical images, the method has potential for *in vivo* medical applications. The model is experimentally verified using magnetic screws moving through a soft-tissue phantom, propelled by a rotating spherical permanent magnet.**

***Index Terms*—Micro/nano robots, medical robots and systems.**

I. Introduction

BIOMEDICAL microrobots hold promise for targeted therapies in the human body. The majority of the research on biomedical microrobots has focused on magnetic swimmers and screws that use some form of chiral structure (e.g., a helix) to convert magnetic torque generated by a rotating magnetic field into forward propulsion (see reviews in [1]–[4]), although it has also been shown that achiral structures can be propelled in a similar fashion [5]. This method of propulsion is inspired by bacterial flagella, and is desirable when critically compared to other methods of magnetic-microrobot propulsion such as sperm-like wiggling or field-gradient-induced pulling [1]. To accomplish a therapeutic task, a large number of such microrobots (i.e., a swarm) will likely be required, and the entire swarm will be subject to some globally applied magnetic field, making it challenging to differentiate actuation between microrobots. In addition, for clinical use, it will be unrealistic to assume that microrobots can be individually localized; rather, a medical image will show a swarm of microrobots as a blob in the image [6]. To date, research on the control of multiple magnetic microrobots has either considered a swarm that is controlled as an aggregate unit with no ability to differentiate microrobots [6]–[8], a small set of heterogeneous microrobots that are individually localized [9]–[19], or a swarm of an arbitrary number of heterogeneous microrobots [20]–[22].

In this letter, we demonstrate how a rotating magnetic dipole field can be used to manipulate a swarm of homogeneous magnetic microrobots (Fig. 1), in terms of its position and shape, using techniques that could realistically be applied to the control of swarms *in vivo*. We characterize the swarm in terms of a mean position (i.e., the centroid of the swarm) with respect to the rotating dipole, and a covariance matrix that describes the shape of the swarm, both of which could be estimated from images. We quantify how these parameters evolve in time and space in a rotating dipole field.

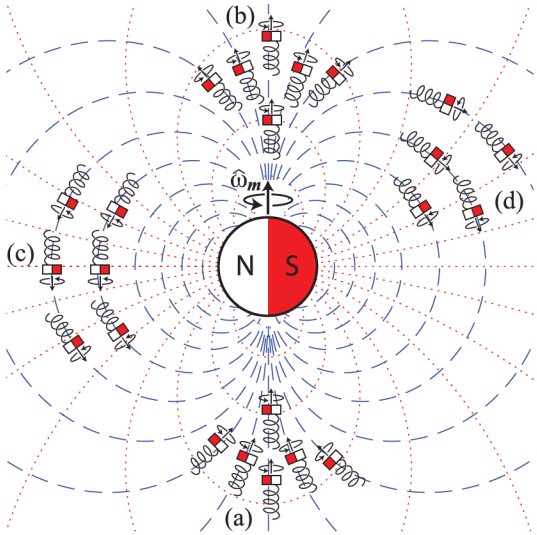

Fig. 1. A magnetic dipole moment $\boldsymbol{m}$ (which points from the south pole to the north pole) generates a magnetic field (⋯), which is radially symmetric about the $\boldsymbol{m}$ axis. If $\boldsymbol{m}$ is rotated about the axis $\hat{\boldsymbol{\omega}}_{\boldsymbol{m}}$, the magnetic field vector $\boldsymbol{b}$ at each location rotates around some axis $\hat{\boldsymbol{\omega}}_{\boldsymbol{b}}$. The streamlines of $\hat{\boldsymbol{\omega}}_{\boldsymbol{b}}$ (– –) are radially symmetric about the $\hat{\boldsymbol{\omega}}_{\boldsymbol{m}}$ axis. Swarms of microrobots are shown at a variety of locations, with microrobots aligned with their respective $\hat{\boldsymbol{\omega}}_{\boldsymbol{b}}$ axes. At locations along the axis $\hat{\boldsymbol{\omega}}_{\boldsymbol{m}}$, swarms are driven straight while either (a) gathering or (b) spreading. At locations that are orthogonal to $\hat{\boldsymbol{\omega}}_{\boldsymbol{m}}$ such as (c), the swarm moves locally straight, tangent to a curved path, but does not gather or spread as it is driven forward. At general locations, such as (d), the swarm will experience both spreading/gathering and steering.

Manuscript received September 10, 2019; accepted January 16, 2020. Date of publication February 10, 2020; date of current version February 20, 2020. This letter was recommended for publication by Associate Editor X. Wu and Editor X. Liu upon evaluation of the reviewers' comments. This work was supported by the National Science Foundation under Awards #1435827 and #1650968. *(Corresponding author: Jake J. Abbott.)*

BhanuKiran Chaluvadi was with the Department of Mechanical Engineering, University of Utah, Salt Lake City, UT 84112 USA, and is now with Blue Ocean Robotics, 5220 Odense SØ, Denmark (e-mail: bhanukiran.chaluvadi@outlook.com).

Kristen M. Stewart, Adam J. Sperry, Henry C. Fu, and Jake J. Abbott are with the Department of Mechanical Engineering, University of Utah, Salt Lake City, UT 84112 USA (e-mail: kristen.stewart@utah.edu; adam.sperry@utah.edu; henry.fu@utah.edu; jake.abbott@utah.edu).

Digital Object Identifier 10.1109/LRA.2020.2972857

II. Kinematics of a Single Microrobot in a Rotating Dipole Field: A Review

A magnetic dipole $\boldsymbol{m}$ (units A·m^2) located at a point $\boldsymbol{P_m}$ generates a magnetic field vector $\boldsymbol{b}$ (units T) at each point $\boldsymbol{P_b}$ described by

$$\boldsymbol{b}\{\boldsymbol{x},\boldsymbol{m}\} = \frac{\mu_0}{4\pi\|\boldsymbol{x}\|^3}\left(3\hat{\boldsymbol{x}}\hat{\boldsymbol{x}}^\top - \mathbb{I}\right)\boldsymbol{m} = \frac{\mu_0}{4\pi\|\boldsymbol{x}\|^3}\mathbb{\Gamma}\{\hat{\boldsymbol{x}}\}\boldsymbol{m}, \tag{1}$$

where $\boldsymbol{x} = \boldsymbol{P_b} - \boldsymbol{P_m}$ (units m) is the relative displacement vector of the point $\boldsymbol{P_b}$ with respect to $\boldsymbol{P_m}$, $\mathbb{I}$ is the identity matrix, $\mu_0 = 4\pi \times 10^{-7}$ T·m/A is the permeability of free space, and we use the "hat" notation to indicate a unit-normalized vector (i.e., $\hat{\boldsymbol{x}} \equiv \boldsymbol{x}/\|\boldsymbol{x}\|$); the vectors can be expressed with respect to any frame, provided they are all expressed with respect to the same frame [23]. The streamlines of the $\boldsymbol{b}$ vector field are depicted in Fig. 1. We see that the magnetic field is nonlinear with respect to position, with a strength that decays rapidly with distance from the source $\propto \|\boldsymbol{x}\|^{-3}$, but the field is linear with respect to the dipole itself. We can use $\mathbb{\Gamma}\{\hat{\boldsymbol{x}}\}$ to capture the shape of the dipole field, which is invariant to distance from the source.

If the dipole moment $\boldsymbol{m}$ is rotated about, and orthogonal to, some axis $\hat{\boldsymbol{\omega}}_{\boldsymbol{m}}$, then the field $\boldsymbol{b}$ at any given point in space will rotate about, and be orthogonal to, some axis $\hat{\boldsymbol{\omega}}_{\boldsymbol{b}}$:

$$\hat{\boldsymbol{\omega}}_{\boldsymbol{b}}\{\boldsymbol{x}\} = (\widehat{\mathbb{\Gamma}^{-1}\{\hat{\boldsymbol{x}}\}\hat{\boldsymbol{\omega}}_{\boldsymbol{m}}}), \tag{2}$$

where

$$\mathbb{\Gamma}^{-1}\{\hat{\boldsymbol{x}}\} = \frac{1}{2}\left(\mathbb{\Gamma}\{\hat{\boldsymbol{x}}\} - \mathbb{I}\right) \tag{3}$$

is always well conditioned [24]. The streamlines of the $\hat{\boldsymbol{\omega}}_{\boldsymbol{b}}$ vector field are depicted in Fig. 1. The dipole and field vectors will rotate with the same period and mean angular velocity, but their instantaneous angular velocities may not be the same in general [24].

If the dipole source, and thus the field, are rotating sufficiently slowly, then the microrobot can be assumed to be rotating synchronously with the field. The body of a microrobot located at $\boldsymbol{P_b}$ will tend to align with $\hat{\boldsymbol{\omega}}_{\boldsymbol{b}}$ as its magnetic element synchronously rotates with $\boldsymbol{b}$, and $\hat{\boldsymbol{\omega}}_{\boldsymbol{b}}$ will become the microrobot's "forward" direction (assuming right-handed chirality). This also assumes that the field is rotated sufficiently slowly to avoid instabilities in which transient torques cause the body of the microrobot to move away from the $\hat{\boldsymbol{\omega}}_{\boldsymbol{b}}$ axis rather than align with it [25]. Under these assumptions, the velocity (units m/s) will be proportional to $\boldsymbol{\omega}_{\boldsymbol{b}}$ (units rad/s) as

$$\boldsymbol{v} = \hat{\boldsymbol{\omega}}_{\boldsymbol{b}} v \tag{4}$$

with an associated speed

$$v \equiv \|\boldsymbol{v}\| = \|\boldsymbol{\omega}_{\boldsymbol{m}}\|\beta, \tag{5}$$

where the coefficient β (units m) is a function of the properties of the fluid environment and the microrobot's geometry [1].

There is a rotation speed $\|\boldsymbol{\omega}_{\boldsymbol{m}}\|$ at which the maximum available magnetic torque is required to keep the microrobot rotating synchronously with the field; this is commonly known as the "step-out frequency" [9]. If the field source is rotated any faster, the speed of the microrobot will reduce, and the linear relationship in (5) will no longer hold [12].

III. Kinematics of a Microrobot Swarm in a Rotating Dipole Field

If we consider a swarm of microrobots at some nominal position, for which the centroid of the swarm ($\boldsymbol{P}_{\bar{\boldsymbol{x}}}$, $\bar{\boldsymbol{x}} = \boldsymbol{P}_{\bar{\boldsymbol{x}}} - \boldsymbol{P_m}$) is the natural choice, we observe that each microrobot will be at a different $\boldsymbol{x}$ and will thus experience a different $\hat{\boldsymbol{\omega}}_{\boldsymbol{b}}$. As shown in Fig. 1, there will be locations in the rotating dipole field in which we can conceive of basic swarm manipulation primitives, such as spreading out or gathering together while moving forward, or steering while moving forward. We first introduced this concept qualitatively in [26]. In this letter, we quantify this phenomenon, using the language of robotic manipulation.

Throughout this letter, we make the assumption that all of the microrobots are rotating synchronously with the applied field, and will consequently all swim with the same speed. This assumption can be enforced by limiting the dipole's rotation frequency to avoid the microrobots entering the step-out or unstable regimes described in Section II.

The swarm itself can be viewed explicitly as a discrete set of N microrobots, or it can be described by a time-varying and spatially varying continuum number density (or concentration) of microrobots $\rho\{\boldsymbol{x},t\}$ (i.e., the number of microrobots per unit volume). Here we will define the centroid, standard deviation, and covariance for both representations, but we will use the continuum approach in our derivation of the swarm kinematics. The centroid of the swarm is its average position,

$$\bar{\boldsymbol{x}}\{t\} = \frac{1}{N}\sum_{i=1}^{N}\boldsymbol{x}_i = \frac{1}{N}\int \boldsymbol{x}\rho\{\boldsymbol{x},t\}\,\mathrm{d}V. \tag{6}$$

The discrete representation can be obtained from the continuum one by using the density $\rho\{\boldsymbol{x},t\} = \sum_{i=1}^{N}\delta\{\boldsymbol{x} - \boldsymbol{x}_i(t)\}$, where $\delta\{\boldsymbol{x}\}$ is the Dirac delta function. The standard deviation in position of the swarm is

$$\sigma = \left(\frac{1}{N}\sum_{i=1}^{N}(\boldsymbol{x}_i - \bar{\boldsymbol{x}})^2\right)^{1/2} = \left(\frac{1}{N}\int(\boldsymbol{x} - \bar{\boldsymbol{x}})^2\rho\{\boldsymbol{x},t\}\,\mathrm{d}V\right)^{1/2}. \tag{7}$$

The standard deviation is a measure of the overall size of the swarm. For example, we would expect 95% of the swarm to fall within a distance of 2σ from the centroid. The covariance $\mathbb{K}$ of the swarm is a 3×3 matrix

$$\begin{aligned}\mathbb{K} &= \frac{1}{N}\sum_{i=1}^{N}(\boldsymbol{x}_i - \bar{\boldsymbol{x}})(\boldsymbol{x}_i - \bar{\boldsymbol{x}})^{\mathsf{T}} \\ &= \frac{1}{N}\int(\boldsymbol{x} - \bar{\boldsymbol{x}})(\boldsymbol{x} - \bar{\boldsymbol{x}})^{\mathsf{T}}\rho\{\boldsymbol{x},t\}\,\mathrm{d}V.\end{aligned} \tag{8}$$

The covariance describes both the size and shape of the swarm. The variance is the trace of the covariance, and the standard deviation (which parameterizes overall size) is the square root of the variance. The square root of the eigenvalues of $\mathbb{K}$ parameterize the extension of the swarm along the corresponding principal axes (i.e., eigenvectors). In the special case of an

isotropic swarm, the eigenvalues are all equal and the covariance is $\mathbb{K} = \sigma^2\mathbb{I}/3$.

Local quantities of the swarm, such as density or orientation, can be characterized using the concept of a *material derivative*, borrowed from continuum fluid mechanics [27]. For any property $Q\{\boldsymbol{x}, t\}$ of an element of material that is moving through space with an instantaneous velocity $\boldsymbol{v}$ (units m/s), the material derivative

$$\frac{DQ}{Dt} \equiv \frac{\partial Q}{\partial t} + (\boldsymbol{v}\cdot\nabla)\,Q \equiv \frac{\partial Q}{\partial t} + \frac{\partial Q}{\partial \boldsymbol{x}}\boldsymbol{v} \tag{9}$$

describes the rate of change in that property moving with the element of material. Q may be scalar-valued (e.g., density) or vector-valued (e.g., velocity). For a vector-valued Q, the element in the ith row and jth column of $\partial Q/\partial \boldsymbol{x}$ is $\partial Q_i/\partial x_j$.

A. Centroid (Mean) of the Swarm

The instantaneous velocity of the centroid of the swarm is the same as the average velocity of the swarm, which, assuming that $\hat{\boldsymbol{\omega}}_{\boldsymbol{b}}$ does not vary appreciably over the size scale of the swarm, is approximately the velocity of a microrobot located at the centroid, as described in (4). See Appendix A for more details.

The instantaneous curvature of the trajectory of the swarm can be found by considering the rate of change of the "forward" direction, moving with the local population:

$$\frac{D\hat{\boldsymbol{\omega}}_{\boldsymbol{b}}}{Dt} = \frac{\partial \hat{\boldsymbol{\omega}}_{\boldsymbol{b}}}{\partial t} + \frac{\partial \hat{\boldsymbol{\omega}}_{\boldsymbol{b}}}{\partial \boldsymbol{x}}\hat{\boldsymbol{\omega}}_{\boldsymbol{b}} v. \tag{10}$$

We are exclusively interested in the motion of a swarm in a "static" rotating dipole field (i.e., where $\boldsymbol{\omega_m}$ is constant), so $\partial\hat{\boldsymbol{\omega}}_{\boldsymbol{b}}/\partial t = \boldsymbol{0}$. We can explicitly compute the spatial derivative of $\hat{\boldsymbol{\omega}}_{\boldsymbol{b}}$ as:

$$\frac{\partial \hat{\boldsymbol{\omega}}_{\boldsymbol{b}}}{\partial \boldsymbol{x}} = \frac{3\left(\mathbb{I} - \hat{\boldsymbol{\omega}}_{\boldsymbol{b}}\hat{\boldsymbol{\omega}}_{\boldsymbol{b}}^{\top}\right)\left(\left(\hat{\boldsymbol{\omega}}_{\boldsymbol{m}}^{\top}\hat{\boldsymbol{x}}\right)\left(\mathbb{I} - 2\hat{\boldsymbol{x}}\hat{\boldsymbol{x}}^{\top}\right) + \hat{\boldsymbol{x}}\hat{\boldsymbol{\omega}}_{\boldsymbol{m}}^{\top}\right)}{2\|\boldsymbol{x}\|\|\mathbb{\Gamma}^{-1}\{\hat{\boldsymbol{x}}\}\hat{\boldsymbol{\omega}}_{\boldsymbol{m}}\|}. \tag{11}$$

This quantity will be important throughout this letter, as it describes how the unit-vector "forward" directions $\hat{\boldsymbol{\omega}}_{\boldsymbol{b}}$ for microrobots throughout the swarm vary relative to $\hat{\boldsymbol{\omega}}_{\boldsymbol{b}}$ at the centroid of the swarm, which is what fundamentally enables us to manipulate the shape of the swarm.

If $D\hat{\boldsymbol{\omega}}_{\boldsymbol{b}}/Dt = \boldsymbol{0}$, the swarm is instantaneously not rotating. Otherwise, the swarm can be considered as traveling on a curved path with an instantaneous curvature (units m^{-1}) defined by

$$\kappa = \frac{1}{r} = \left\| \frac{\partial \hat{\boldsymbol{\omega}}_{\boldsymbol{b}}}{\partial \boldsymbol{x}}\hat{\boldsymbol{\omega}}_{\boldsymbol{b}} \right\| \tag{12}$$

where r (units m) is the instantaneous radius of curvature.

B. Swarm Density/Concentration

To determine if a swarm of microrobots is spreading or gathering (see Fig. 1), one can examine the rate of change in density (concentration) moving with that swarm (i.e., the material derivative of the density):

$$\frac{D\rho}{Dt} = \frac{\partial \rho}{\partial t} + (v\hat{\boldsymbol{\omega}}_{\boldsymbol{b}}\cdot\nabla)\rho. \tag{13}$$

Since $\rho\boldsymbol{v}$ is the flux of microrobots, by conservation of number, the number density ρ obeys:

$$\begin{aligned}\frac{\partial \rho}{\partial t} &= -\nabla\cdot(\rho\boldsymbol{v}) = -\nabla\cdot(\rho v\hat{\boldsymbol{\omega}}_{\boldsymbol{b}}) \\ &= -\rho(\nabla\cdot\hat{\boldsymbol{\omega}}_{\boldsymbol{b}})v - (v\hat{\boldsymbol{\omega}}_{\boldsymbol{b}}\cdot\nabla)\rho,\end{aligned} \tag{14}$$

which is analogous to the relation between mass flux and mass density [27]. Therefore, (13) can be written as

$$\frac{D\rho}{Dt} = -\rho(\nabla\cdot\hat{\boldsymbol{\omega}}_{\boldsymbol{b}})v = -\mathrm{tr}\left\{\frac{\partial\hat{\boldsymbol{\omega}}_{\boldsymbol{b}}}{\partial\boldsymbol{x}}\right\}v\rho, \tag{15}$$

where the trace of $\partial\hat{\boldsymbol{\omega}}_{\boldsymbol{b}}/\partial\boldsymbol{x}$ can be efficiently computed (i.e., without explicitly computing $\partial\hat{\boldsymbol{\omega}}_{\boldsymbol{b}}/\partial\boldsymbol{x}$) as

$$\mathrm{tr}\left\{\frac{\partial\hat{\boldsymbol{\omega}}_{\boldsymbol{b}}}{\partial\boldsymbol{x}}\right\} = \frac{3\left(\hat{\boldsymbol{\omega}}_{\boldsymbol{m}}^{\top}\hat{\boldsymbol{x}}\left(1 + 2\left(\hat{\boldsymbol{\omega}}_{\boldsymbol{b}}^{\top}\hat{\boldsymbol{x}}\right)^2\right) - \hat{\boldsymbol{\omega}}_{\boldsymbol{b}}^{\top}\hat{\boldsymbol{x}}\hat{\boldsymbol{\omega}}_{\boldsymbol{m}}^{\top}\hat{\boldsymbol{\omega}}_{\boldsymbol{b}}\right)}{2\|\boldsymbol{x}\|\|\mathbb{\Gamma}^{-1}\{\hat{\boldsymbol{x}}\}\hat{\boldsymbol{\omega}}_{\boldsymbol{m}}\|}. \tag{16}$$

A positive (negative) value of $D\rho/Dt$ indicates an increasing (decreasing) population density, which corresponds to a gathering (spreading) of microrobots.

We may be more interested in the relative change in the density, rather than the absolute value of the density. In that case, we will consider the material derivative of the density normalized by the instantaneous density:

$$\frac{1}{\rho}\frac{D\rho}{Dt} = -\mathrm{tr}\left\{\frac{\partial\hat{\boldsymbol{\omega}}_{\boldsymbol{b}}}{\partial\boldsymbol{x}}\right\}v. \tag{17}$$

C. Swarm Shape (Covariance)

The rate of change of the covariance $\mathbb{K}$ can be computed directly from the spatial derivative of $\hat{\boldsymbol{\omega}}_{\boldsymbol{b}}$ evaluated at the centroid of the swarm:

$$\frac{\partial\mathbb{K}}{\partial t} = \left(\mathbb{K}\left(\frac{\partial\hat{\boldsymbol{\omega}}_{\boldsymbol{b}}}{\partial\boldsymbol{x}}\right)^{\top} + \frac{\partial\hat{\boldsymbol{\omega}}_{\boldsymbol{b}}}{\partial\boldsymbol{x}}\mathbb{K}^{\top}\right)v, \tag{18}$$

The derivation of (18), provided in Appendix A, assumes that the swarm is sufficiently small to linearize $\hat{\boldsymbol{\omega}}_{\boldsymbol{b}}$ about the centroid of the swarm.

D. Overall Swarm Size (Standard Deviation)

The time derivative of the standard deviation $\sigma = \sqrt{\mathrm{tr}\{\mathbb{K}\}}$ can be found using the chain rule

$$\frac{\partial\sigma}{\partial t} = \frac{1}{2\sqrt{\mathrm{tr}\{\mathbb{K}\}}}\mathrm{tr}\left\{\frac{\partial\mathbb{K}}{\partial t}\right\} = \frac{v}{\sigma}\mathrm{tr}\left\{\mathbb{K}\left(\frac{\partial\hat{\boldsymbol{\omega}}_{\boldsymbol{b}}}{\partial\boldsymbol{x}}\right)^{\top}\right\}, \tag{19}$$

which for an isotropic swarm ($\mathbb{K} = \sigma^2\mathbb{I}/3$) simplifies to

$$\frac{\partial\sigma}{\partial t} = \mathrm{tr}\left\{\frac{\partial\hat{\boldsymbol{\omega}}_{\boldsymbol{b}}}{\partial\boldsymbol{x}}\right\}\frac{v\sigma}{3}. \tag{20}$$

This result can also be rationalized from the rate of change of density, (13). For a swarm of N microrobots in a volume V, we

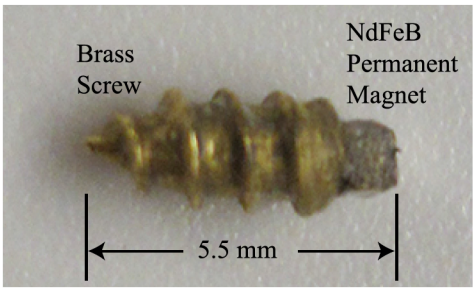

Fig. 2. Magnetic screw.

expect the density to scale as $\rho \propto \frac{N}{V} \propto \frac{N}{\sigma^3}$. As a result,

$$\frac{1}{\rho}\frac{D\rho}{Dt} = \frac{-3}{\sigma}\frac{\partial \sigma}{\partial t}, \tag{21}$$

which when combined with (17) yields (20).

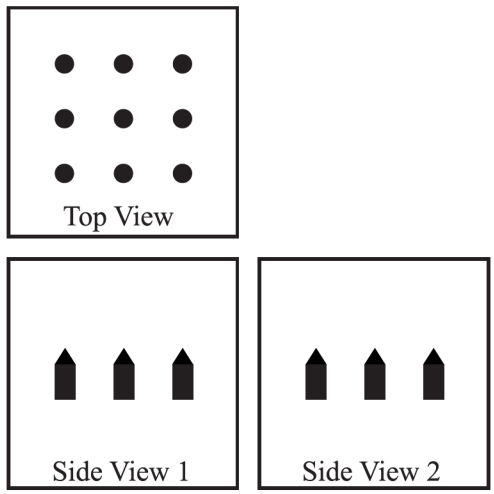

Fig. 3. Depiction of how the nine magnetic screws are initialized in the agar gel inside the cubic container, and what the two cameras capture in orthogonal side views.

IV. Experimental Verification

The "microrobots" used in our experiments each comprise a No. 2 brass wood screw with the head removed and replaced with a cubic NdFeB N50-grade permanent magnet with a side length of 1 mm (Fig. 2). The magnet was selected as to not exceed the minor diameter of the screw thread. The dipole of the magnet is oriented orthogonal to the screw axis. Each magnetic screw is measured to be 5.5 mm in length.

The soft-tissue phantom used in the experiment is an agar gel prepared by boiling a mixture of agar powder and water at double strength for one minute. The mixture is diluted to the final concentration of 0.5 wt% agar, poured into a transparent cubic container, and refrigerated for 12 hours. Nine magnetic screws are placed approximately vertically into the agar gel to form a swarm (Fig. 3). For one experiment (gathering) the magnetic screws are initialized near the bottom of the container with their tips pointing upward, and for the other two experiments (spreading and straight motion) the magnetic screws are initialized near the top of the container with their tips pointing downward.

For our magnetic-dipole-field source, we use the spherical-actuator-magnet manipulator (SAMM) [28]. The SAMM uses three mutually orthogonal omniwheels to continuously rotate a 51-mm-diameter spherical NdFeB permanent magnet, with dipole moment $\|\boldsymbol{m}\| = 71.6$ A·m^2, about arbitrary axes. A robotic arm is used to position the magnet.

We perform three experiments—gathering, spreading, and locally straight motion—corresponding to Figs. 1a–1c, respectively; these experiments are shown in Figs. 4–6, respectively. In the experiments, the SAMM is placed either above or adjacent to the container that contains the swarm. The relatively slow rotation speeds of the SAMM magnet were chosen during pilot testing to ensure that no step-out or unstable behaviors of the screws were observed; these should not be interpreted as maximum achievable speeds. Two cameras are placed at orthogonal side views (see Fig. 3) to record the motion of the screws, which were driven open-loop (i.e., the images were not used in closed-loop control). Although the screws are started approximately vertically, it is evident how they rotate themselves into alignment with their local $\hat{\boldsymbol{\omega}}_{\boldsymbol{b}}$ directions (see video attachment).

Figs. 4–6 also depict the results of the open-loop kinematic model, verifying that the model is a good approximation of the evolution of the swarm, suitable for use as an *a priori* model for motion planners and feedback control systems. A pilot test with a single magnetic screw was used to determine the β value relating rotation rate to forward velocity, which was then utilized by the model for all subsequent experiments. Before each experiment, the initial position of the centroid of the swarm (i.e., the magnet of the central magnetic screw) was measured with respect to the center of the SAMM magnet. A covariance matrix was selected such that the planar projections of a corresponding ellipsoid onto the two orthogonal views visually surrounded the initial swarm (with principal-axis dimensions equal to the square root of the eigenvalues of the covariance matrix). Then, during each experiment, the swarm model was evolved open-loop (see video attachment).

V. Discussion

In this letter, we have described the physical process by which a single rotating magnetic dipole field can be used to manipulate a microrobot swarm. If the manipulation workspace is surrounded by multiple sources, or a movable source, such motions will be possible in multiple, possibly arbitrary, directions. Determining how many field sources are required and where they should be placed, for general and application-specific tasks, is left as an open question.

The dipole model (1) approximates the fields of all magnetic sources at sufficient distance [23]. It accurately describes the field of spherical permanent magnets, such as that of the SAMM, at all locations. It can also be quite accurate for compact permanent-magnet geometries (e.g., cubes, certain cylinders) at

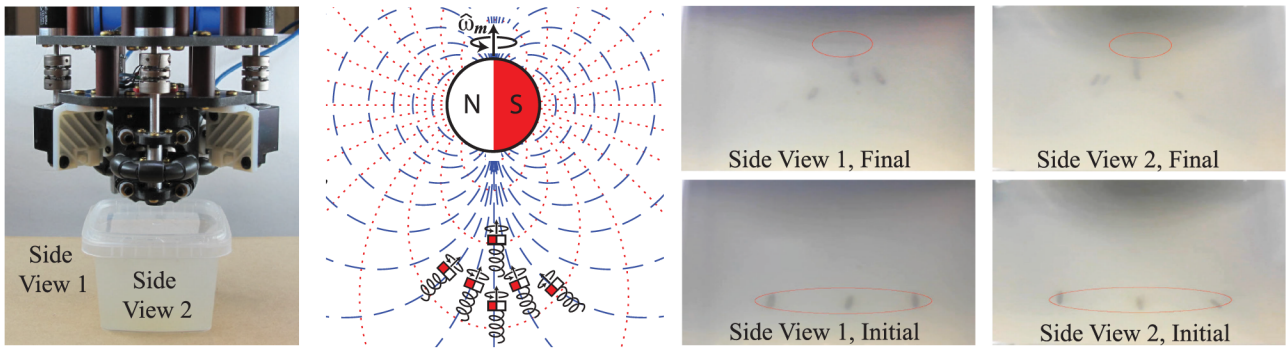

Fig. 4. Typical results for gathering. The centroid of the swarm is initially at $\bar{\boldsymbol{x}} = [0\ 0\ -90]^{\mathsf{T}}$ mm. The SAMM magnet is rotated with $\|\boldsymbol{\omega_m}\| = 0.31$ rad/s about the positive vertical axis, causing the screws to move upward (toward the SAMM magnet). The red ellipsoid shows the open-loop kinematic model, which is initialized to match the swarm.

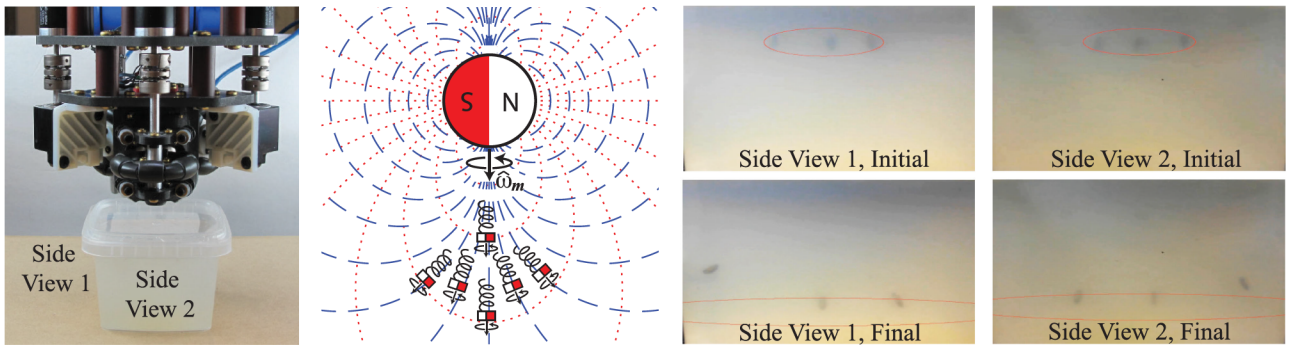

Fig. 5. Typical results for spreading. The centroid of the swarm is initially at $\bar{\boldsymbol{x}} = [0\ 0\ -65]^{\mathsf{T}}$ mm. The SAMM magnet is rotated with $\|\boldsymbol{\omega_m}\| = 0.50$ rad/s about the negative vertical axis, causing the screws to move downward (away from the SAMM magnet). The red ellipsoid shows the open-loop kinematic model, which is initialized to match the swarm.

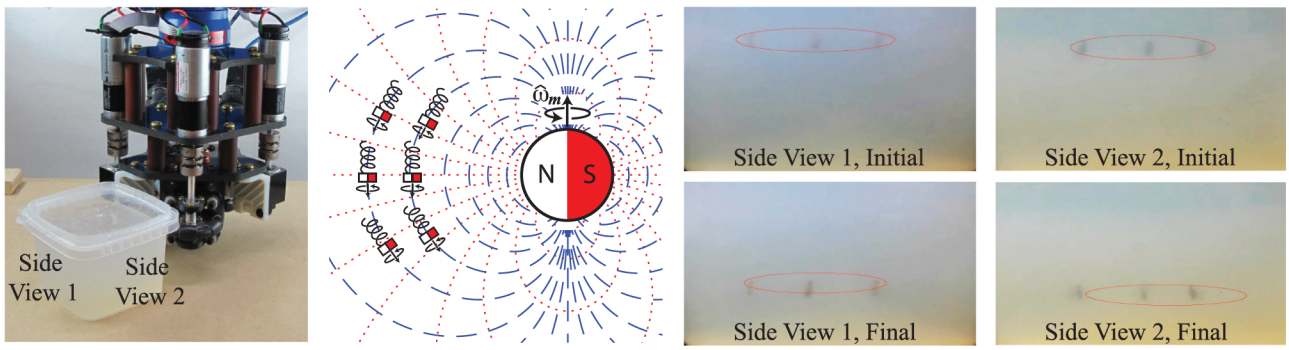

Fig. 6. Typical results for locally straight motion. The centroid of the swarm is initially at $\bar{\boldsymbol{x}} = [0\ -48\ 5]^{\mathsf{T}}$ mm. The SAMM magnet is rotated with $\|\boldsymbol{\omega_m}\| = 0.19$ rad/s about the positive vertical axis, causing the screws to move downward (antiparallel to $\hat{\boldsymbol{\omega}}_{\boldsymbol{m}}$). The red ellipsoid shows the open-loop kinematic model, which is initialized to match the swarm.

clinically relevant distances [29]. In addition, our group has developed electromagnetic field sources that were optimized to generate a field that is accurately modeled by the dipole model [30].

We note that for each of the kinematic parameters of interest, the time rate of change of the parameter is linearly proportional to the parameter itself. It is also linearly proportional to the speed of the microrobots, which is in turn proportional to the rotation speed of the rotating dipole-field source (provided rotations speeds are kept sufficiently slow).

We note that the magnitude of the elements in $\partial\hat{\boldsymbol{\omega}}_{\boldsymbol{b}}/\partial\boldsymbol{x}$ (which appears in every kinematic equation of interest except the velocity of the centroid) decay uniformly with distance from the source $\propto \|\boldsymbol{x}\|^{-1}$. Thus, the use of spatial changes in the rotating dipole field, as proposed in this letter, becomes more difficult with increasing distance. Because the dipole field model

of a magnetic source places the dipole at the center of the source, this scaling problem cannot be circumvented simply by constructing a larger magnetic source. However, constructing a larger magnetic source will lead to stronger fields at a given distance from the surface of the source, which will enable higher microrobot speeds.

We have assumed that each microrobot in the swarm is independent, interacting with the applied field of the rotating dipole, but not interacting with each other. However, magnetic and fluidic interactions will certainly exist [7], [31], [32]. Vach *et al.* [15] estimate that the unmodeled interactions for this type of microrobot will be negligible for microrobots separated by at least five body lengths, but they conjecture that models which assume independence may retain sufficient validity with denser packing. We have also assumed that the effects of magnetic torque dominate the magnetic actuation of the microrobots. In practice, periodic magnetic forces will be present [33], [34], acting as a disturbance on velocity. These forces will become smaller relative to the torques of interest with increasing distance from the dipole source [23]. Finally, the kinematic models do not include a transient response as the microrobots align themselves with the $\hat{\boldsymbol{\omega}}_{\boldsymbol{b}}$ vectors, which will lead to inaccuracies if $\hat{\boldsymbol{\omega}}_{\boldsymbol{m}}$ changes rapidly.

The kinematic model assumes that the microrobots are always aligned with their local $\hat{\boldsymbol{\omega}}_{\boldsymbol{b}}$ vectors, which is likely to be a quite accurate assumption for microrobots swimming in fluid. However, for microrobots moving through soft tissue, as in our experiments, the magnetic torque attempting to align the microrobots with their local $\hat{\boldsymbol{\omega}}_{\boldsymbol{b}}$ vectors is opposed by the environment. As a result, the model overpredicts the steering. This is evident in the open-loop models in our experiments, which always overpredict the change in the swarm covariance. The model also sometimes overpredicts the velocity of the swarm. This is due to the fact that the kinematic model assumes no step-out behavior or slipping (e.g., tearing of the soft tissue), which will always tend to reduce the velocity from that predicted by the model. It is possible that a correction factor could be included, for a given microrobot swarm in a given soft tissue, to improve the model's predicting power; such a correction factor would likely be found experimentally, or could be learned in real time. However, closing the control loop with periodic image-based feedback should be the ultimate goal.

In the future, it may be possible to exploit the step-out regime, as has been done in uniform fields [12], [22], to differentiate the speed of the microrobots as a function of their position in the swarm, which would enable another means for swarm manipulation beyond what we have characterized here. This and other swarm-manipulation concepts using a rotating dipole field are proposed in [26].

VI. Conclusion

In this letter, we showed how a rotating magnetic dipole field will manipulate the location (i.e., centroid), shape (i.e., covariance, standard deviation), and density of a swarm of magnetic microrobots that convert rotation into forward propulsion (e.g., helical swimmers and screws). The result of this letter is a kinematic model that can be used as an *a priori* model for motion planners and feedback control systems. Because the model is fully three-dimensional and does not require any localization information beyond what could realistically be determined from medical images, the method has potential for *in vivo* medical applications.

Appendix A
Derivation of Centroid Velocity and Eq. (18)

Throughout this appendix we use Einstein (indicial) notation, which greatly simplifies the calculus to that of scalar quantities. This means that we describe vectors and matrices by their elements. For example, the ith element of vector $\boldsymbol{x}$ is denoted x_i, and the element of matrix $\mathbb{A}$ in the ith row and jth column is denoted A_{ij}.

In terms of elements, the 3×3 matrix product $\mathbb{A} = \mathbb{B}\mathbb{C}$ is expressed as

$$A_{ij} = \sum_{k=1}^{3} B_{ik} C_{kj}. \tag{22}$$

We further simplify expressions by removing the summation and assuming that a summation is implied if a particular index (in this case k) appears more than once in a product of terms. Thus we write the matrix product $\mathbb{A} = \mathbb{B}\mathbb{C}$ in full Einstein notation as

$$A_{ij} = B_{ik} C_{kj}, \tag{23}$$

where the summation is implied because k appears twice in the product.

Now consider a swarm described by number density $\rho\{\boldsymbol{x}, t\}$. We assume that the swarm is finite in size and small compared to the length scales over which $\hat{\boldsymbol{\omega}}_{\boldsymbol{b}}$ varies. The position of the swarm is described by its centroid $\bar{\boldsymbol{x}}$, computed in terms of its components as

$$\bar{x}_i = \frac{1}{N} \int x_i \rho\{\boldsymbol{x}, t\} \mathrm{d}V, \tag{24}$$

where N is the total number of microrobots. The bar denotes averaging over the swarm distribution. We can compute the time evolution of the centroid by using (14):

$$\partial_t \bar{x}_i = \frac{1}{N} \int x_i (\partial_t \rho)\, \mathrm{d}V = -\frac{1}{N} \int x_i \partial_k \left[\rho v \hat{\boldsymbol{\omega}}_{\boldsymbol{b},k}\right] \mathrm{d}V, \tag{25}$$

where $\hat{\boldsymbol{\omega}}_{\boldsymbol{b},k}$ is the kth element of $\hat{\boldsymbol{\omega}}_{\boldsymbol{b}}$, ∂_t is the partial derivative with respect to time, and ∂_k represents the partial derivative with respect to x_k. Integrating by parts and discarding the boundary term, which vanishes since the density is zero at infinity, we obtain

$$\partial_t \bar{x}_i = \frac{1}{N} \int (\partial_k x_i) \left[\rho v \hat{\boldsymbol{\omega}}_{\boldsymbol{b},k}\right] \mathrm{d}V = \frac{1}{N} \int \rho v \hat{\boldsymbol{\omega}}_{\boldsymbol{b},i} \mathrm{d}V = v \overline{\hat{\boldsymbol{\omega}}}_{\boldsymbol{b},i}. \tag{26}$$

Thus the centroid moves with the average velocity of the distribution, as expected. By Taylor expanding the velocity field around the centroid,

$$v \hat{\boldsymbol{\omega}}_{\boldsymbol{b}} \approx v \hat{\boldsymbol{\omega}}_{\boldsymbol{b}}\{\bar{\boldsymbol{x}}\} + (x_k - \bar{x}_k) v [\partial_k \hat{\boldsymbol{\omega}}_{\boldsymbol{b}}\{\bar{\boldsymbol{x}}\}], \tag{27}$$

we see that the average velocity is equal to the velocity evaluated at the centroid, up to first order in the expansion:

$$\begin{aligned} v\overline{\hat{\boldsymbol{\omega}}_{\boldsymbol{b},i}} &= \frac{1}{N}\int \rho v[\hat{\boldsymbol{\omega}}_{\boldsymbol{b},i}\{\bar{\boldsymbol{x}}\}]\mathrm{d}V \\ &\quad + \frac{1}{N}\int \rho v\left[(x_k-\bar{x}_k)[\partial_k\hat{\boldsymbol{\omega}}_{\boldsymbol{b},i}\{\bar{\boldsymbol{x}}\}]+\cdots\right]\mathrm{d}V \\ &= v\hat{\boldsymbol{\omega}}_{\boldsymbol{b},i}\{\bar{\boldsymbol{x}}\} + v(\bar{x}_k-\bar{x}_k)[\partial_k\hat{\boldsymbol{\omega}}_{\boldsymbol{b},i}\{\bar{\boldsymbol{x}}\}]+\cdots \\ &= v\hat{\boldsymbol{\omega}}_{\boldsymbol{b},i}\{\bar{\boldsymbol{x}}\}+\cdots \end{aligned} \tag{28}$$

In indicial notation, the elements of $\mathbb{K}$ can be computed as

$$\begin{aligned} K_{ij} &= \frac{1}{N}\int (x_i-\bar{x}_i)(x_j-\bar{x}_j)\rho\{\boldsymbol{x},t\}\mathrm{d}V \\ &= \overline{(x_i-\bar{x}_i)(x_j-\bar{x}_j)} = \overline{x_ix_j}-\bar{x}_i\bar{x}_j. \end{aligned} \tag{29}$$

The time evolution of $\mathbb{K}$ is then

$$\begin{aligned} \partial_t K_{ij} &= \frac{1}{N}\int x_ix_j(\partial_t\rho)\,\mathrm{d}V - (\partial_t\bar{x}_i)\bar{x}_j - \bar{x}_i(\partial_t\bar{x}_j) \\ &= -\frac{1}{N}\int x_ix_j\partial_k\left[\rho v\hat{\boldsymbol{\omega}}_{\boldsymbol{b},k}\right]\mathrm{d}V - v\overline{\hat{\boldsymbol{\omega}}_{\boldsymbol{b},i}}\bar{x}_j - \bar{x}_iv\overline{\hat{\boldsymbol{\omega}}_{\boldsymbol{b},j}}. \end{aligned} \tag{30}$$

To compute the first term of the last expression, integrate by parts to obtain

$$\begin{aligned} \partial_t\overline{x_ix_j} &= -\frac{1}{N}\int x_ix_j\partial_k\left[\rho v\hat{\boldsymbol{\omega}}_{\boldsymbol{b},k}\right]\mathrm{d}V \\ &= \frac{1}{N}\int \partial_k(x_ix_j)\left[\rho v\hat{\boldsymbol{\omega}}_{\boldsymbol{b},k}\right]\mathrm{d}V \\ &= \frac{1}{N}\int x_j\left[\rho v\hat{\boldsymbol{\omega}}_{\boldsymbol{b},i}\right]+x_i\left[\rho v\hat{\boldsymbol{\omega}}_{\boldsymbol{b},j}\right]\mathrm{d}V. \end{aligned} \tag{31}$$

Expanding $\hat{\boldsymbol{\omega}}_{\boldsymbol{b}} \approx \hat{\boldsymbol{\omega}}_{\boldsymbol{b}}\{\bar{\boldsymbol{x}}\} + (x_k-\bar{x}_k)\partial_k\hat{\boldsymbol{\omega}}_{\boldsymbol{b}}\{\bar{\boldsymbol{x}}\}$,

$$\begin{aligned} &\frac{1}{N}\int x_j\left[\rho v\hat{\boldsymbol{\omega}}_{\boldsymbol{b},i}\right]\mathrm{d}V \\ &= \frac{1}{N}\int x_j\left[\rho v\hat{\boldsymbol{\omega}}_{\boldsymbol{b},i}\{\bar{\boldsymbol{x}}\}\right]\mathrm{d}V \\ &\quad + \frac{1}{N}\int x_j(x_k-\bar{x}_k)\left[\rho v(\partial_k\hat{\boldsymbol{\omega}}_{\boldsymbol{b},i}\{\bar{\boldsymbol{x}}\})\right]\mathrm{d}V \\ &= \bar{x}_jv\hat{\boldsymbol{\omega}}_{\boldsymbol{b},i}\{\bar{\boldsymbol{x}}\} + \left[\overline{x_jx_k}-\bar{x}_j\bar{x}_k\right]\left[v(\partial_k\hat{\boldsymbol{\omega}}_{\boldsymbol{b},i}\{\bar{\boldsymbol{x}}\})\right]. \end{aligned} \tag{32}$$

Substituting this into (31),

$$\begin{aligned} \partial_t\overline{x_ix_j} = {}& \bar{x}_jv\hat{\boldsymbol{\omega}}_{\boldsymbol{b},i} + \left[\overline{x_jx_k}-\bar{x}_j\bar{x}_k\right]\left[v(\partial_k\hat{\boldsymbol{\omega}}_{\boldsymbol{b},i})\right] \\ &+ \bar{x}_iv\hat{\boldsymbol{\omega}}_{\boldsymbol{b},j} + \left[\overline{x_ix_k}-\bar{x}_i\bar{x}_k\right]\left[v(\partial_k\hat{\boldsymbol{\omega}}_{\boldsymbol{b},j})\right] \end{aligned} \tag{33}$$

with all quantities evaluated at the centroid of the swarm $\bar{\boldsymbol{x}}$. Now substituting (33) into (30), and using (28),

$$\begin{aligned} \partial_tK_{ij} = {}& \left[\overline{x_ix_k}-\bar{x}_i\bar{x}_k\right]\left[v(\partial_k\hat{\boldsymbol{\omega}}_{\boldsymbol{b},j})\right] \\ &+ \left[\overline{x_jx_k}-\bar{x}_j\bar{x}_k\right]\left[v(\partial_k\hat{\boldsymbol{\omega}}_{\boldsymbol{b},i})\right] \\ = {}& K_{ik}vJ_{kj} + K_{jk}vJ_{ki} \end{aligned} \tag{34}$$

where $J_{kj} = \frac{\partial\hat{\boldsymbol{\omega}}_{\boldsymbol{b},j}}{\partial\boldsymbol{x}_k}$ are the components of (11) such that $\mathbb{J}^\top = \partial\hat{\boldsymbol{\omega}}_{\boldsymbol{b}}/\partial\boldsymbol{x}$ evaluated at the centroid of the swarm.

REFERENCES

[1] J. J. Abbott *et al.*, "How should microrobots swim?" *Int. J. Robot. Res.*, vol. 28, no. 11/12, pp. 3663–3667, 2009.

[2] B. J. Nelson, I. K. Kaliakatsos, and J. J. Abbott, "Microrobots for minimally invasive medicine," *Annu. Rev. Biomed. Eng.*, vol. 12, pp. 55–85, 2010.

[3] E. Diller *et al.*, "Micro-scale mobile robotics," *Found. Trends Rob.*, vol. 2, no. 3, pp. 143–259, 2013.

[4] M. Sitti, *Mobile Microrobotics*. Cambridge, MA, USA: MIT Press, 2017.

[5] U. K. Cheang, F. Meshkati, D. Kim, M. J. Kim, and H. C. Fu, "Minimal geometric requirements for micropropulsion via magnetic rotation," *Phys. Rev. E*, vol. 90, 2014, Art. no. 033007.

[6] A. Servant, F. Qiu, M. Mazza, K. Kostarelos, and B. J. Nelson, "Controlled in vivo swimming of a swarm of bacteria-like microrobotic flagella," *Adv. Mater.*, vol. 27, no. 19, pp. 2981–2988, 2015.

[7] S. Tottori, L. Zhang, K. E. Peyer, and B. J. Nelson, "Assembly, disassembly, and anomalous propulsion of microscopic helices," *Nano Lett.*, vol. 13, no. 9, pp. 4263–4268, 2013.

[8] P. J. Vach, S. Klumpp, and D. Faivre, "Pattern formation and collective effects in populations of magnetic microswimmers," *J. Phys. D: Appl. Phys.*, vol. 49, 2016, Art. no. 065003.

[9] K. Ishiyama, M. Sendoh, and K. I. Arai, "Magnetic micromachines for medical applications," *J. Magn. Magn. Mater.*, vol. 242, pp. 41–46, 2002.

[10] S. Tottori, N. Sugita, R. Kometani, S. Ishihara, and M. Mitsuishi, "Selective control method for multiple magnetic helical microrobots," *J. Micro-Nano Mechatronics*, vol. 6, no. 3-4, pp. 89–95, 2011.

[11] U. K. Cheang, K. Lee, A. A. Julius, and M. J. Kim, "Multiple-robot drug delivery strategy through coordinated teams of microswimmers," *Appl. Phys. Lett.*, vol. 105, no. 8, 2014, Art. no. 083705.

[12] A. W. Mahoney, N. D. Nelson, K. E. Peyer, B. J. Nelson, and J. J. Abbott, "Behavior of rotating magnetic microrobots above the step-out frequency with application to control of multi-microrobot systems," *Appl. Phys. Lett.*, vol. 104, no. 14, 2014, Art. no. 144101.

[13] E. Diller, J. Giltinan, and M. Sitti, "Independent control of multiple magnetic microrobots in three dimensions," *Int. J. Robot. Res.*, vol. 32, no. 5, pp. 614–631, 2013.

[14] N. D. Nelson and J. J. Abbott, "Generating two independent rotating magnetic fields with a single magnetic dipole for the propulsion of untethered magnetic devices," in *Proc. IEEE Int. Conf. Robot. Autom.*, 2015, pp. 4056–4061.

[15] P. J. Vach, D. Walker, P. Fischer, P. Fratzl, and D. Faivre, "Steering magnetic micropropellers along independent trajectories," *J. Phys. D: Appl. Phys.*, vol. 50, 2017, Art. no. 11LT03.

[16] A. Becker, C. Onyuksel, T. Bretl, and J. McLurkin, "Controlling many differential-drive robots with uniform control inputs," *Int. J. Robot. Res.*, vol. 33, no. 13, pp. 1626–1644, 2014.

[17] T. Bretl, "Minimum-time optimal control of many robots that move in the same direction at different speeds," *IEEE Trans. Robot.*, vol. 28, no. 2, pp. 351–363, 2012.

[18] P. Mandal, V. Chopra, and A. Ghosh, "Independent positioning of magnetic nanomotors," *ACS Nano*, vol. 9, no. 5, pp. 4717–4725, 2015.

[19] J. Rahmer, C. Stehning, and B. Gleich, "Spatially selective remote magnetic actuation of identical helical micromachines," *Sci. Robot.*, vol. 2, no. 3, 2017, Art. no. eaal2845.

[20] P. J. Vach *et al.*, "Selecting for function: Solution synthesis of magnetic nanopropellers," *Nano Lett.*, vol. 13, pp. 5373–5378, 2013.

[21] D. Schamel, M. Pfeifer, J. G. Gibbs, B. Miksch, A. G. Mark, and P. Fischer, "Chiral colloidal molecules and observation of the propeller effect," *J. Am. Chem Soc.*, vol. 135, pp. 12 353–12 359, 2013.

[22] T. A. Howell, B. Osting, and J. J. Abbott, "Sorting rotating micromachines by variations in their magnetic properties," *Phys. Rev. Appl.*, vol. 9, 2018, Art. no. 054021.

[23] J. J. Abbott, E. Diller, and A. J. Petruska, "Magnetic methods in robotics," *Annu. Rev. Cont. Robot. Autom.*, vol. 3, pp. 2.1–2.34, 2020.

[24] A. W. Mahoney and J. J. Abbott, "Generating rotating magnetic fields with a single permanent magnet for propulsion of untethered magnetic devices in a lumen," *IEEE Trans. Robot.*, vol. 30, no. 2, pp. 411–420, Apr. 2014.

[25] A. W. Mahoney, N. D. Nelson, E. M. Parsons, and J. J. Abbott, "Non-ideal behaviors of magnetically driven screws in soft tissue," in *Proc. IEEE/RSJ Int. Conf. Intell. Robot. Syst.*, 2012, pp. 3559–3564.

[26] J. J. Abbott and H. C. Fu, "Controlling homogeneous microrobot swarms in vivo using rotating magnetic dipole fields," in *Proc. 18th Int. Symp. ISRR Robot. Res. Springer Proc. Adv. Robot.*, Springer, 2020, vol. 10, pp. 3–8.

[27] P. Kunda, I. Cohen, and D. Dowling, *Fluid Mechanics*, 6th ed. New York, NY, USA: Academic, 2015.

[28] S. E. Wright, A. W. Mahoney, K. M. Popek, and J. J. Abbott, "The spherical-actuator-magnet manipulator: A permanent-magnet robotic end-effector," *IEEE Trans. Robot.*, vol. 33, no. 5, pp. 1013–1024, Oct. 2017.

[29] A. J. Petruska and J. J. Abbott, "Optimal permanent-magnet geometries for dipole field approximation," *IEEE Trans. Magn.*, no. 2, pp. 811–819, Feb. 2013.

[30] A. J. Petruska and J. J. Abbott, "Omnimagnet: An omnidirectional electromagnet for controlled dipole-field generation," *IEEE Trans. Magn.*, vol. 50, no. 7, 2014, Art. no. 8400810.

[31] U. K. Cheang, F. Meshkati, H. Kim, K. Lee, H. C. Fu, and M. J. Kim, "Versatile microrobotics using simple modular subunits," *Sci. Rep.*, vol. 6, 2016, Art. no. 30472.

[32] J. Yu, T. Xu, Z. Lu, C. I. Vong, and L. Zhang, "On-demand disassembly of paramagnetic nanoparticle chains for microrobotic cargo delivery," *IEEE Trans. Robot.*, vol. 33, no. 5, pp. 1213–1225, Oct. 2017.

[33] A. W. Mahoney and J. J. Abbott, "Managing magnetic force applied to a magnetic device by a rotating dipole field," *Appl. Phys. Lett.*, vol. 99, 2011, Art. no. 134103.

[34] A. W. Mahoney, S. E. Wright, and J. J. Abbott, "Managing the attractive magnetic force between an untethered magnetically actuated tool and a rotating permanent magnet," in *Proc. IEEE Int. Conf. Robot. Autom.*, 2013, pp. 5346–5351.